

A series of dithienobenzodithiophene based small molecules for highly efficient organic solar cells

Huanran Feng¹, Miaomiao Li¹, Wang Ni¹, Bin Kan^{1,2}, Yunchuang Wang^{1,2}, Yamin Zhang¹, Hongtao Zhang^{1,2*}, Xiangjian Wan^{1,2} & Yongsheng Chen^{1,2*}

¹Centre of Nanoscale Science and Technology and Key Laboratory of Functional Polymer Materials, State Key Laboratory and Institute of Elemento-Organic Chemistry, Collaborative Innovation Center of Chemical Science and Engineering (Tianjin), College of Chemistry, Nankai University, Tianjin 300071, China

²School of Materials Science and Engineering, National Institute for Advanced Materials, Nankai University, Tianjin 300071, China

Received November 9, 2016; accepted December 7, 2016; published online February 27, 2017

Three acceptor-donor-acceptor (A-D-A) small molecules DCAODTBDT, DRDTBDT and DTBDTBDT using dithieno[2,3-d:2',3'-d']benzo[1,2-b:4,5-b']dithiophene as the central building block, octyl cyanoacetate, 3-octylrhodanine and thiobarbituric acid as the end groups were designed and synthesized as donor materials in solution-processed photovoltaic cells (OPVs). The impacts of these different electron withdrawing end groups on the photophysical properties, energy levels, charge carrier mobility, morphologies of blend films, and their photovoltaic properties have been systematically investigated. OPVs device based on DRDTBDT gave the best power conversion efficiency (PCE) of 8.34%, which was significantly higher than that based on DCAODTBDT (4.83%) or DTBDTBDT (3.39%). These results indicate that rather dedicated and balanced consideration of absorption, energy levels, morphology, mobility, etc. for the design of small-molecule-based OPVs (SM-OPVs) and systematic investigations are highly needed to achieve high performance for SM-OPVs.

acceptor-donor-acceptor, dithieno[2,3-d:2',3'-d']benzo[1,2-b:4,5-b']dithiophene, solution-processed photovoltaic cells, end acceptor moieties

Citation: Feng H, Li M, Ni W, Kan B, Wang Y, Zhang Y, Zhang H, Wan X, Chen Y. A series of dithienobenzodithiophene based small molecules for highly efficient organic solar cells. *Sci China Chem*, 2017, 60: 552–560, doi: 10.1007/s11426-016-0461-1

1 Introduction

Organic photovoltaic cells (OPVs) have been considered to be one of the most promising candidates for the next generation energy sources due to their advantages of low cost, light-weight, solution processability, and flexibility [1,2]. In the past decade, there has been tremendous progress in the performance of this technology owing to the development of new electron-donor [3–7] and electron-acceptor

materials [8–10], improved device geometries, and metal/organic interfaces [11–16]. Currently, power conversion efficiencies (PCEs) over 10% have been achieved for polymer-based OPVs (P-OPVs) with bulk heterojunction (BHJ) device structure [17–22]. Compared with P-OPVs, solution processed small-molecule-based OPVs (SM-OPVs) have attracted more and more attention benefiting from their definite but versatile chemical structures and well-reproducible device performances. To date, the highest PCEs of solution processed SM-OPVs have also been over 10%, which is comparable to the performance of P-OPVs [23–27].

To further improve the PCE and for the commercialization

*Corresponding authors (email: htzhang@nankai.edu.cn; yschen99@nankai.edu.cn)

of OPVs, innovation of photoactive materials is still an important and necessary approach for both polymer based and small molecule based OPVs. For the design of donor materials, it is necessary to strike a delicate balance between broad and intense absorption, suitable energy levels, high mobility, good solubility and film-forming property. Successful strategies for designing donor molecules involve combination of electron-rich (D) moieties and electron-deficient (A) moieties in A-D-A or D-A-D systems [28,29]. As one type of push-pull structures, the A-D-A type molecule architecture can effectively tune the highest occupied molecular orbitals (HOMO) and lowest unoccupied molecular orbitals (LUMO) levels, lower the band gap (E_g) and extend the absorption through changing the central building blocks and end moieties [30,31]. With this strategy, tremendous efforts have been made for A-D-A type small molecules and PCEs over 9%–10% have been achieved [24–27,32,33].

Among various photovoltaic materials for the application in OPVs, fused aromatic units with planar conjugated backbones are particularly interesting due to their well delocalized π -conjugation along the backbones [34–37]. The benzo[1,2-b:4,5-b'] dithiophene (BDT) unit has been widely used as an attractive donor building block for donor materials used in high performance OPVs due to its large and rigid planar conjugated structure [38–41]. Furthermore, linearly fused derivatives of BDT, such as dithieno[2,3-d:2',3'-d']benzo[1,2-b:4,5-b']dithiophene (DTBDT), as donor units in polymers have also shown high performance. [42,43] The DTBDT unit with an enlarged planar area can enhance the electron delocalization and promote cofacial π - π stacking in the solid state, rendering the films to have superior intermolecular charge-transport properties. Thus, DTBDT derivatives have been widely used as building blocks in conjugated molecules for application in high-performance organic field effect transistors (OFET) and P-OPVs [36,43–45]. However, only a very few studies on DTBDT-based small molecule photovoltaic materials have been reported, which afforded relatively low PCEs (4.35% and 4.98%) [46,47].

In parallel with the investigation on electron-rich central units (D), it has been demonstrated that the terminal electron-deficient units (A) also have a great influence on the absorption, energy levels, mobilities and final solar cell performances of the corresponding molecules [30,48]. Thus different electron withdrawing units, such as alkyl cyanoacetate, rhodanine and thiobarbituric acid have been widely investigated and are well performed when introduced into A-D-A type molecules because of their capability of effectively inducing intramolecular charge transfer and enhancing optical absorption [31,49–52].

With this in mind and based on our previous work, we herein report the synthesis and characterization of three DTBDT derivatives with different end groups

(DCAODTBDT, DRDTBDT and DTBDTBDT) as shown in Scheme 1 for solution processed SM-OPV. The impacts of these different end acceptor moieties on the photophysical properties, the energy levels of HOMO and LUMO, charge carrier mobility, the morphologies of blend films, and their photovoltaic properties are systematically investigated. Among them, DRDTBDT shows a PCE as high as 8.34%, which is the highest value reported for DTBDT-based SM-OPVs.

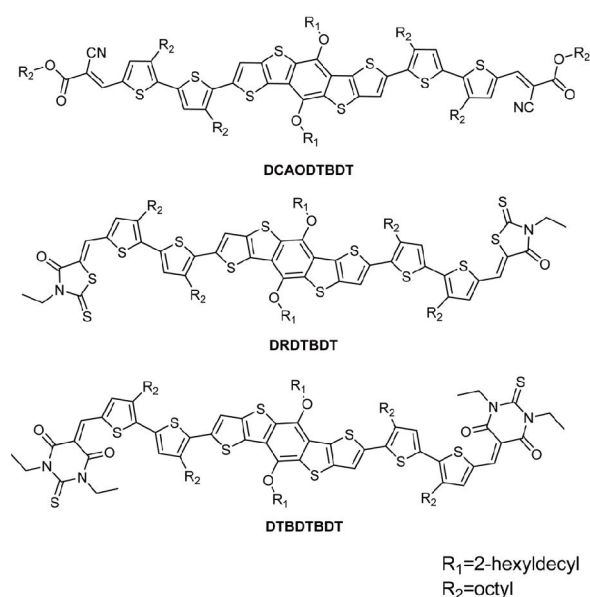
2 Experimental

2.1 Synthesis

Detailed synthetic schemes for the three materials can be found in the Supporting Information online. All reactions and manipulations were carried out under argon atmosphere with the use of standard Schlenk techniques. All starting materials, unless otherwise specified, were purchased from commercial suppliers and used without further purification. (5,10-Bis((2-hexyldecyl)oxy)dithieno[2,3-d:2',3'-d']benzo[1,2-b:4,5-b']dithiophene-2,7-diyl)bis-(trimethylstannane) was prepared following the literature method [45].

2.2 Measurements and instruments

The ^1H and ^{13}C nuclear magnetic resonance (NMR) spectra were taken on a Bruker AV400 Spectrometer (Germany). Matrix assisted laser desorption/ionization time-of-flight mass spectrometry (MALDI-TOF MS) was performed on a Bruker Autoflex III instrument (Germany). Transmission



Scheme 1 Chemical structures of DCAODTB, DRDTBDT and DTBDTBDT.

electron microscopy (TEM) was performed on a Philips Technical G2 F20 (Netherlands) at 200 kV. Thermogravimetric analyses (TGA) were carried out on a NETZSCH STA 409PC instrument (Germany) under a purified nitrogen gas flow with a 10 °C min⁻¹ heating rate. UV-Vis spectra were obtained with a JASCO V-570 spectrophotometer (Japan). The grazing incidence wide angle X-ray scattering (GIWAXS) samples were prepared on PEDOT:PSS-coated Si substrates using the same preparation conditions as for devices. Resonant soft X-ray scattering (RSoXS) was performed at beamline 11.0.1.2 Lawrence Berkeley National Lab. A 284.2 eV beamline energy at PCBM k-edge was chosen to enhance the contrast. Cyclic voltammetry (CV) experiments were performed with a LK98B II Microcomputer-based electrochemical analyzer in dichloromethane solutions. All measurements were carried out at room temperature with a conventional three-electrode configuration using a glassy carbon electrode as the working electrode, a saturated calomel electrode (SCE) as the reference electrode, and a Pt wire as the counter electrode. The dichloromethane was distilled from calcium hydride under dry argon immediately prior to use tetrabutylammonium phosphorus hexafluoride (Bu₄NPF₆, 0.1 M) in dichloromethane was used as the supporting electrolyte, and the scan rate was 100 mV s⁻¹.

The current density-voltage (*J-V*) characteristics of photovoltaic devices were obtained by a Keithley 2400 (USA) source-measure unit. The photocurrent was measured under simulated illumination of 100 mW cm⁻² with AM 1.5G irradiation using a xenon-lamp-based solar simulator (Oriel 96000 (AM 1.5G)) in an argon-filled glove box. Simulator irradiance was characterized using a calibrated spectrometer, and illumination intensity was set using a certified silicon diode. External quantum efficiency values (EQEs) of the encapsulated devices were obtained with a halogen-tungsten lamp, monochromator, optical chopper, and lock-in amplifier in air and the photon flux was determined by a calibrated silicon photodiode.

SCLC mobility was measured using a diode configuration of ITO/PEDOT:PSS/donor:PC₇₁BM/Au for hole mobility and ITO/Al/donor:PC₇₁BM/Al for electron mobility by taking the dark current density in the range of 0–6 V and fitting the results to a space charge limited form, where SCLC is described by:

$$J = \frac{9\epsilon_r\epsilon_0\mu_0 V^2}{8L^3}$$

where *J* is the current density, *L* is the film thickness of the active layer, μ_0 is the mobility, ϵ_r is the relative dielectric constant of the transport medium, ϵ_0 is the permittivity of free space (8.85 × 10⁻¹² F m⁻¹), *V* (= *V*_{appl} - *V*_{bi}) is the internal voltage in the device, in which *V*_{appl} is the applied voltage to the device and *V*_{bi} is the built-in voltage due to the relative work function difference of the two electrodes.

2.3 Fabrication of photovoltaic cells

The photovoltaic devices were fabricated with a structure of glass/ITO/PEDOT:PSS/donor:acceptor/PrC60MA/Al. The ITO-coated glass substrates were cleaned by ultrasonic treatment in detergent, deionized water, acetone, and isopropyl alcohol under ultrasonication for 15 min each time and subsequently dried by a nitrogen flow. A thin layer of PEDOT:PSS (Baytron P VP Al 4083, filtered at 0.45 μm) was spin-coated (3000 r min⁻¹, ca. 40 nm thick) onto the ITO surface. After baked at 150 °C for 20 min, the substrates were transferred into an argon-filled glove box. Subsequently, the active layer was spin-coated from blend chloroform solutions with the weight ratio of donor and PC₇₁BM at 1:0.8 and then the substrates were placed in a glass petri dish containing 200 μL chloroform for 90 s for solvent vapor annealing (DRDTBDT and DTBDBDT) or on the heating plate performed thermal annealing at 100 °C for 10 min. PrC60MA solution (0.5 mg mL⁻¹, dissolved in methanol) was spin-coated at 3000 r min⁻¹, a 50 nm Al layer was deposited on the PrC60MA film under high vacuum (<1 × 10⁻⁴ Pa) with a deposition rate of 0.5 Å s⁻¹. The effective area of each cell was 4 mm² as defined by shadow masks for the solar cell devices discussed in this work.

3 Results and discussion

3.1 Synthesis and thermal stability of the compounds

The synthesis procedures of DCAODTBDT, DRDTBDT and DTBDBDT were shown in Scheme S1 (Supporting Information online). (5,10-Bis((2-hexyldecyl-oxy)dithieno[2,3-d:2',3'-d']benzo[1,2-b:4,5-b']dithiophene-2,7-diyl)bis(trimethylstannane) (compound **1**) was prepared following the literature method [45]. DCHOTBDT was synthesized by the Still coupling reaction between compound **1** and 5'-bromo-3,4'-dioctyl-2,2'-bithiophene-5-carbaldehyde (compound **2**) under argon atmosphere in the presence of Pd(PPh₃)₄ as the catalyst for 24 h. The target molecules were obtained by Knoevenagel condensation of their corresponding acceptor moieties octyl cyanoacetate, 3-octylrhodanine and thiobarbituric acid with DCHODTBDT in the presence of pyridine or trimethylamine. The thermal stability of these compounds was investigated by TGA (Figure S1, Supporting Information online). The results reveal that the onset decomposition temperatures of the compounds are all around 330 °C under N₂ atmosphere, indicating that they are quite thermally stable and can be used for device fabrication.

3.2 Optical absorption and electrochemical properties

The optoelectronic properties of DCAODTBDT, DRDTBDT and DTBDBDT were characterized using UV-Vis absorption. Figure 1 shows the absorption spectra of these three

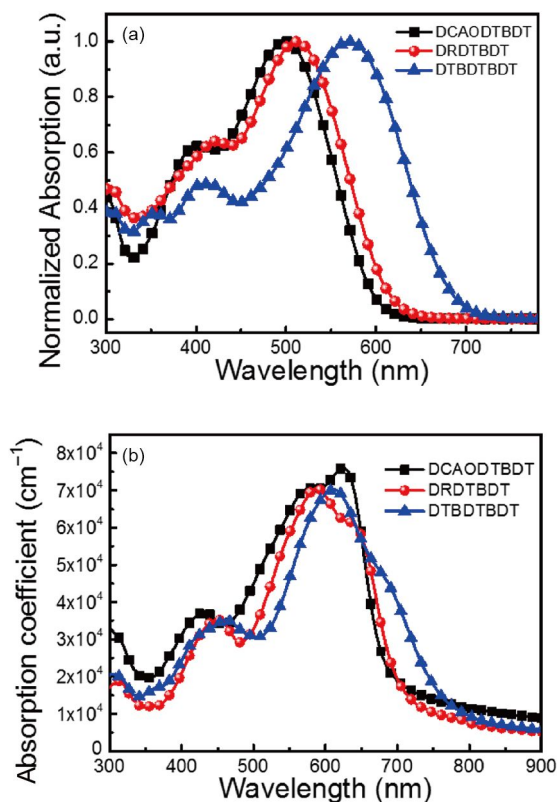


Figure 1 Absorption spectra of DCAODTBDT, DRDTBDT and DTBDTBDT in (a) chloroform solution and (b) the as-cast films (color online).

molecules in chloroform solution and in the solid state. The detailed absorption data, including the absorption maximum in solution and film as well as the optical band gap are summarized in Table 1. DCAODTBDT, DRDTBDT and DTBDTBDT exhibit maximum absorption peak at 500, 512 and 570 nm in solutions, respectively. In the solid state, DCAODTBDT and DRDTBDT display a large red-shifted (79 and 77 nm) and obvious vibronic shoulder peak with their solution absorption, while DTBDTBDT shows a relatively smaller red-shifted of 42 nm and much weak shoulder peak, probably because of its weak intermolecular packing. In addition, the much high vibronic peak at 624 nm of DCAODTBDT indicates effective π - π stacking between molecular backbones. By extrapolation of the absorption onsets in the film state, the optical band gap of DCAODTBDT, DRDTBDT and DTBDTBDT are estimated to be 1.82, 1.75 and 1.58 eV, respectively.

The electrochemical properties of DCAODTBDT,

DRDTBDT and DTBDTBDT were investigated by CV. Ferrocene/ferrocenium of the (Fc/Fc⁺) redox couple (4.8 eV below the vacuum level) was used as the internal calibration. As shown in Figure 2, the energy levels of LUMO, which are -3.22 eV for DCAODTBDT, -3.32 eV for DRDTBDT, and -3.57 eV for DTBDTBDT, respectively, were calculated from the onset oxidation and reduction potential (Table 1). All the molecules exhibit very similar HOMO energy levels (-5.04 to -5.05 eV), which is predominantly determined by the donor moiety. In contrast to the HOMO levels, the LUMO levels of these three molecules changed distinctly, leading to different bandgaps of these molecules from 1.82 to 1.48 eV, due to the different end groups. Generally, for A-D-A small molecules, the HOMO energy levels are mainly decided by the central donor segments, and the LUMO energy levels are more related to the terminal acceptor segments. These electrochemical and optical data demonstrated that the band gap and absorption spectra of these A-D-A type molecules can be tuned effectively through the introduction of different acceptor terminal units as we discussed previously [53,54], and the electron withdrawing ability of these acceptor units is in the order of thiobarbituric acid > rhodanine > 2-ethylhexyl cyanoacetate [50,54].

3.3 Photovoltaic performance

Bulk heterojunction organic solar cells were fabricated using DCAODTBDT, DRDTBDT and DTBDTBDT as the electron donor materials and [6,6]-phenyl-C₇₁-butyric acid methyl ester (PC₇₁BM) as the electron acceptor material with a device structure of glass/ITO/PEDOT:PSS/donor:acceptor/ETL-1/Al, using the conventional solution spin-coating process, and tested under AM 1.5G illumination at an intensity of 100 mW cm⁻². ETL-1 is a methanol-soluble fullerene-surfactant developed by Jen *et al.* [55], and its structure is shown in Figure S2. The optimum *J-V* curves with a donor:acceptor ratio of 1:0.8 (*w/w*) are shown in Figure 2. The detailed photovoltaic parameters are given in Table 2. The device based on DRDTBDT without post treatment showed only a PCE of 1.97%, with an open-circuit voltage (*V*_{oc}) of 0.93 V, a short-circuit current density (*J*_{sc}) of 6.45 mA cm⁻², and a fill factor (FF) of 33%. The device based on DTBDTBDT:PC₇₁BM exhibited a *V*_{oc} of 0.95 V, a *J*_{sc} of 4.50 mA cm⁻², and a FF of 26%, also resulting in a low PCE of 1.13%. Compared with the poor performance of DRDTBDT and DTBDTBDT, DCAODTBDT based device

Table 1 Optical and electrochemical data of DCAODTBDT, DRDTBDT and DTBDTBDT

Compound	$\lambda_{\max, \text{sol}}$ (nm)	ϵ_{sol} (L mol ⁻¹ cm ⁻¹)	$\lambda_{\max, \text{film}}$ (nm)	HOMO ^{CV} (eV)	LUMO ^{CV} (eV)	E_g^{CV} (eV)
DCAODTBDT	500	7.3×10^4	579, 624	-5.04	-3.22	1.82
DRDTBDT	512	8.5×10^4	589, 639	-5.04	-3.32	1.72
DTBDTBDT	570	9.2×10^4	612	-5.05	-3.57	1.48

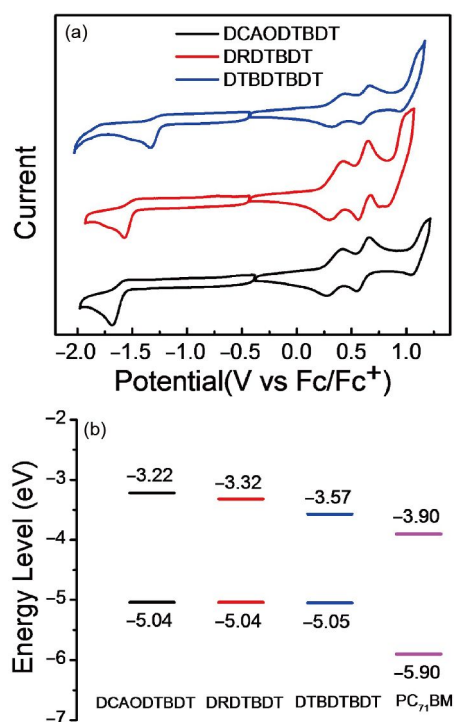


Figure 2 (a) Cyclic voltammograms of DCAODTBDT, DRDTBDT and DTBDTBDT in dichloromethane solutions with $0.1 \text{ mol L}^{-1} \text{ Bu}_4\text{NPF}_6$ and a scan rate of 100 mV s^{-1} ; (b) electronic energy level diagram of DCAODTBDT, DRDTBDT, DTBDTBDT and PC_{71}BM [42] (color online).

exhibited a moderate PCE of 4.20%. The low J_{sc} and FF of the devices were attributed to the un-optimized morphologies of the photovoltaic layers, which could be seen from the TEM images and RSoXS discussed below. DRDTBDT and DTBDTBDT based devices exhibited the best performance after solvent vapor annealing (SVA) and DCAODTBDT based devices exhibit the best performance under thermal annealing at $100 \text{ }^\circ\text{C}$ for 10 min. Except for DTBDTBDT with annealing, all the other devices exhibit close values of V_{oc} (0.90–0.95 V), which is in line with the close HOMO energy levels of these molecules. The device based on DRDTBDT with SVA treatment showed significantly improved J_{sc} of 13.74 mA cm^{-2} and FF of 67%, thus resulting in a significantly higher PCE of 8.34%. This is among the highest values for dithienobenzodithiophene based organic

solar cells. DCAODTBDT based device exhibits a V_{oc} of 0.94 V, a J_{sc} of 8.38 mA cm^{-2} , and a FF of 61%, resulting in a moderate PCE of 4.83%. For the DTBDTBDT based device, SVA treatment also improved the OPV performance with enhanced J_{sc} and FF, yielded a PCE of 3.39%.

The EQE curves of the best devices based on DCAODTBDT, DRDTBDT and DTBDTBDT are shown in Figure 3(b). The DTBDTBDT exhibited the broadest response across the wavelength range of 300–800 nm with the maximum EQE value reaching 66% at 470 nm. The devices based on DRDTBDT showed slightly narrower photovoltaic response in long wavelength range but comparatively higher quantum efficiency (73% at 510 nm) than the devices based on DTBDTBDT. On the other hand, the DCAODTBDT-based device exhibited the lowest EQE with a maximum of 50% at 470 nm, in agreement with its low J_{sc} value in the device. The calculated J_{sc} values integrated from the EQE curves showed 3%–5% mismatch compared with the J_{sc} values obtained from the devices J - V curves.

To further understand the significant differences of performance for the three molecules, the relationship between the photocurrent (J_{ph}) and effective voltage (V_{eff}) was measured. As shown in Figure 3(c), the results are plotted as the dependence of the photocurrent density J_{ph} ($J_{\text{ph}}=J_{\text{L}}-J_{\text{D}}$) on the effective voltage V_{eff} ($V_{\text{eff}}=V_0-V_a$), in which J_{L} and J_{D} are the current densities under illumination and in the dark, respectively, V_a is the applied voltage, and V_0 is the voltage at which $J_{\text{ph}}=0$ [56,57]. For DRDTBDT-based devices, J_{ph} has a nearly linear dependence on the voltage at a low value of V_{eff} , and J_{ph} reaches saturation (where saturation current density J_{sat} was obtained) when the effective voltage V_{eff} arrives at a relatively low voltage of 1.7 V. This suggests that for DRDTBDT-based device, both the processes of photo-generated excitons dissociation into free charge and the charge collection at the electrodes are more efficient with little geminate and bimolecular recombination. Compared with DRDTBDT, DCAODTBDT-based devices show higher saturation V_{eff} with lower J_{ph} due to fewer charges are collected. For the DTBDTBDT case, the J_{ph} does not saturate even at $V_{\text{eff}}=3 \text{ V}$ and increases with higher bias, suggesting a significant geminate and bimolecular recombination or less efficient interfacial contact, thus a lower FF [58–60]. The ratio of $J_{\text{ph}}/J_{\text{sat}}$ can be used to judge

Table 2 Photovoltaic performance of the devices based on DCAODTBDT, DRDTBDT and DTBDTBDT ^{a)}

Donor	V_{oc} (V)	J_{sc} (mA cm^{-2})	FF (%)	PCE (%)
DCAODTBDT ^{b)}	0.91 ± 0.01 (0.92)	7.93 ± 0.12 (8.06)	0.55 ± 0.01 (0.56)	4.06 ± 0.13 (4.20)
DCAODTBDT ^{c)}	0.93 ± 0.01 (0.94)	8.14 ± 0.24 (8.38)	0.60 ± 0.01 (0.61)	4.60 ± 0.20 (4.83)
DRDTBDT ^{b)}	0.92 ± 0.01 (0.93)	6.20 ± 0.23 (6.45)	0.32 ± 0.01 (0.33)	1.79 ± 0.15 (1.97)
DRDTBDT ^{d)}	0.89 ± 0.01 (0.90)	13.40 ± 0.28 (13.74)	0.66 ± 0.01 (0.67)	8.25 ± 0.11 (8.34)
DTBDTBDT ^{b)}	0.94 ± 0.01 (0.95)	4.30 ± 0.17 (4.50)	0.25 ± 0.01 (0.26)	1.07 ± 0.15 (1.13)
DTBDTBDT ^{d)}	0.82 ± 0.01 (0.83)	10.00 ± 0.12 (10.12)	0.39 ± 0.01 (0.40)	3.21 ± 0.18 (3.39)

a) Average values calculated from >20 devices with the standard deviation for the measurements. The best PCEs are provided in parentheses. b) Without post treatment. c) With thermal annealing at $120 \text{ }^\circ\text{C}$ for 10 min. d) With solvent vapor annealing for 90 s.

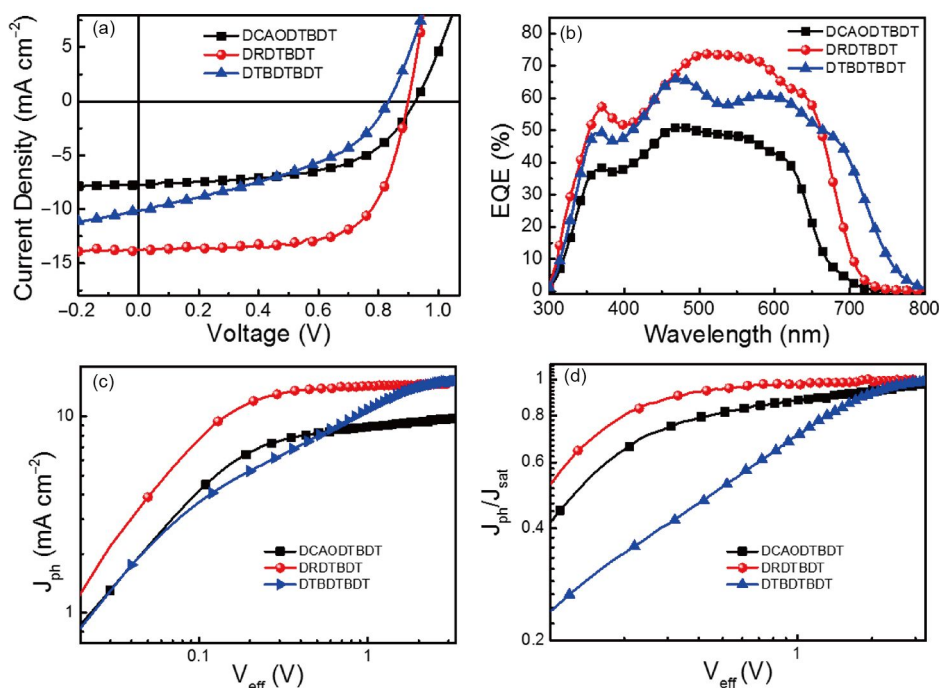


Figure 3 Device performance with structure ITO/PEDOT:PSS/donor:PC₇₁BM/ETL-1/Al. (a) Characteristic current density versus voltage (J - V) curves of both devices under optimized conditions and simulated AM 1.5G irradiation (100 mW cm^{-2}); (b) EQE curves for both devices; (c, d) photocurrent density and charge collection efficiency versus effective voltage (V_{eff}) characteristics for both devices under constant incident light intensity (AM 1.5G, 100 mW cm^{-2}) (color online).

the overall exciton dissociation efficiency and charge collection efficiency [61]. The values of $J_{\text{ph}}/J_{\text{sat}}$ are 87%, 96% and 66% for DCAODTBDT, DRDTBDT and DTBDTBDT-based devices, respectively, under the short circuit conditions. At the maximal power output conditions, the values of $J_{\text{ph}}/J_{\text{sat}}$ are 71%, 82% and 38% for these three molecules, respectively. These results indicate that the device with DRDTBDT possesses higher exciton dissociation efficiency and charge collection efficiency, thus achieving enhanced OPV performance [61]. On the other hand, the much lower $J_{\text{ph}}/J_{\text{sat}}$ of DTBDTBDT may indicate the existence of much more bimolecular recombination, which usually leads to a low FF. In addition, under optimized conditions, the DRDTBDT-based device has a larger shunt resistance ($775 \Omega \text{ cm}^{-2}$) than for DCAODTBDT ($538 \Omega \text{ cm}^{-2}$) and DTBDTBDT ($142 \Omega \text{ cm}^{-2}$), and small series resistance ($5.3 \Omega \text{ cm}^{-2}$) among these three molecules, suggesting a better ohmic contact is formed in the DRDTBDT-based device.

3.4 Morphology and mobility

To gain a deeper understanding of the effect of the end group changes of the dithienobenzodithiophene based small molecules on their photovoltaic characteristics, the blend morphology and crystalline ordering of the DCAODTBDT:PC₇₁BM, DRDTBDT:PC₇₁BM and DTBDTBDT:PC₇₁BM films were investigated by GIWAXS, TEM and RSoXS.

As shown in Figure 4, the microstructures of DCAODTBDT, DRDTBDT and DTBDTBDT blend films with PC₇₁BM as cast and under the optimized conditions were investigated by GIWAXS measurements. All of the three molecules had pronounced (100) scattering peaks in the out-of-plane direction with lamellar spacings of 23.3 \AA ($q=0.27 \text{ \AA}^{-1}$, where q is the scattering vector), 21.6 \AA ($q=0.29 \text{ \AA}^{-1}$) and 20.3 \AA ($q=0.31 \text{ \AA}^{-1}$) for DCAODTBDT, DRDTBDT and DTBDTBDT blend films at the optimized device conditions, respectively (Table 3). DCAODTBDT:PC₇₁BM and DRDTBDT:PC₇₁BM exhibited clear (100), (200) and even (300) diffractions in the direction of out-of-plane, indicating a long-range order and crystallinity in the blend film under two conditions. On the other hand, DRDTBDT blend film show only relative weak (100) diffraction as cast and with post treatment, which implies much less long range lamellar packing and ordering. In addition, DCAODTBDT:PC₇₁BM exhibited clear out-of-plane (010) reflection out-of-plane both at 1.74 \AA^{-1} at the optimized device conditions, corresponding to a π - π stacking distance of 3.61 \AA . However, DTBDTBDT:PC₇₁BM showed no out-of-plane (010) diffraction even after post treatment, though a weak in-plane (010) diffraction corresponding to a d spacing of 3.81 \AA observed at the optimized condition (Figure S4). As can be seen in Table 3, DCAODTBDT and DRDTBDT blend film have the shorter π - π stacking distance than DTBDTBDT, which indicates the formation of denser

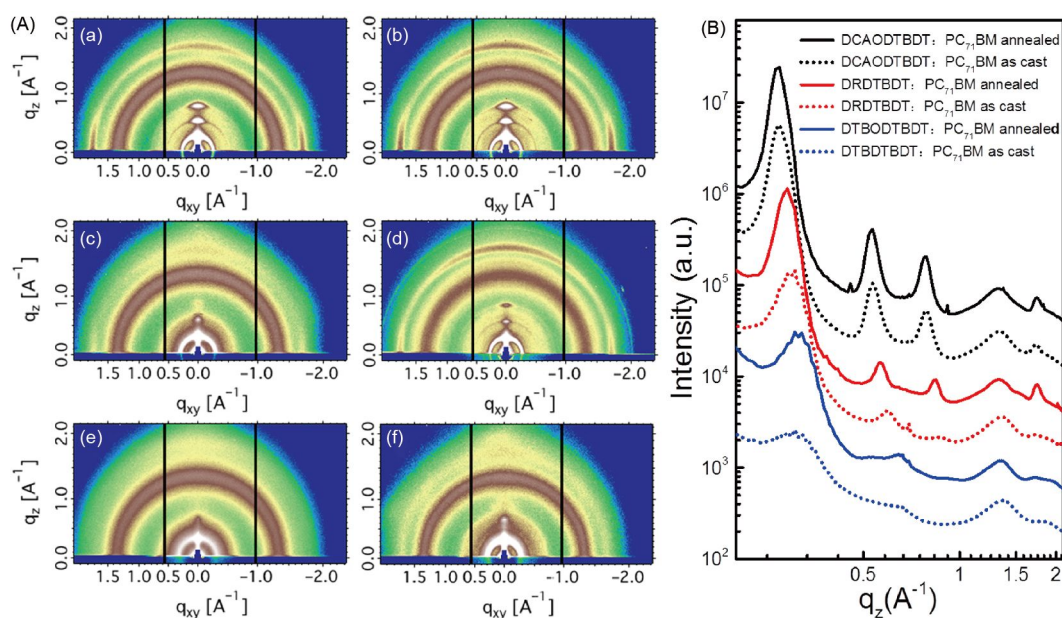


Figure 4 (A) GIWAXS images of (a, b) DCAODTBDT:PC₇₁BM (1:0.8, w/w), (c, d) DRDTBDT:PC₇₁BM (1:0.8, w/w) and (e, f) DTBDTBDT:PC₇₁BM (1:0.8, w/w) blend films from CHCl₃. (a, c, e) The blend films without post treatment; (b, d, f) the blend films with treatment. (B) Out-of-plane line cut profiles of GIWAXS pattern without treatment and with post treatment for the blend films (color online).

Table 3 Morphological data of GIWAXS and RSoXS under optimized conditions

Blends	(100) Out-of-plane		(010) In-plane		RSoXS	
	q (\AA^{-1})	d (\AA)	q (\AA^{-1})	d (\AA)	q (\AA^{-1})	Center-to-center distance (nm)
DCAODTBDT	0.27	23.3	1.74	3.61	0.0055	114
DRDTBDT	0.29	21.6	1.74	3.61	0.0146	43
DTBDTBDT	0.31	20.3	3.61	3.81	0.0120	52

interchain packing. As we can see, although these molecules have the same central building block dithienobenzodithiophene, different molecule packings are achieved. It is most likely due to the different acceptors which can significantly affect packing orders of molecules as we have discussed [50,53,54].

TEM image studies show that the morphologies of the blend films for these three molecules are quite different. As for DCAODTBDT blend film, the TEM images indicate that the dissatisfactory solar cell performance is in some degree relevant to the low quality of morphology of the blend film with PC₇₁BM, whose domain size is as large as 80 nm. Furthermore, the domain size does not change a lot after post treatment, which would lead to low efficient exciton separation, charge transport, and thus lower FF and J_{sc} . Both of DRDTBDT:PC₇₁BM and DTBDTBDT:PC₇₁BM blend films exhibited rather uniform and even distributed domains (20–30 nm) without post treatment. After SVA treatment, the DRDTBDT:PC₇₁BM blend film exhibited bicontinuous interpenetrating networks with well-developed fibrillary structure, and the widths of the fibrils were less than 20 nm. This would be beneficial for exciton diffusion/dissociation and charge transport, thus leads to a high J_{sc} and FF [62].

For the DTBDTBDT:PC₇₁BM blend film, neither clear interpenetrating network or no nanoscale fibrillary features are observed, though there is some extent of phase separation appeared after annealing. RSoXS was employed to further study the thin film morphology, which provided a better statistics of the size of phase separation. As shown in Figure 5, without post treatment, only DCAODTBDT:PC₇₁BM blend film shows an interference ($q=0.0051 \text{ \AA}^{-1}$) corresponding to a domain center-to-center distance of 123 nm, and DTBDTBDT blend film shows a much weak and broad reflection at 0.0358 \AA^{-1} corresponding to a domain center-to-center distance of 17.5 nm. After treatment, the blend films show well-defined scattering peaks at 0.0055, 0.0146 and 0.0120 \AA^{-1} , which are corresponding to distance to 114, 43 and 52 nm, respectively (Table 3). Note that one-half of this center-to-center distance is close to the ideal exciton diffusion distance. These results are consistent with the morphological results measured by TEM, indicating a more favorable exciton diffusion/dissociation in DRDTBDT devices. In addition, although the DTBDTBDT blend film shows a fine interferences characteristic of a phase separated morphology with a size scale of 52 nm, the amorphous nature of DTBDTBDT made it hard to transport electrons and, thus the

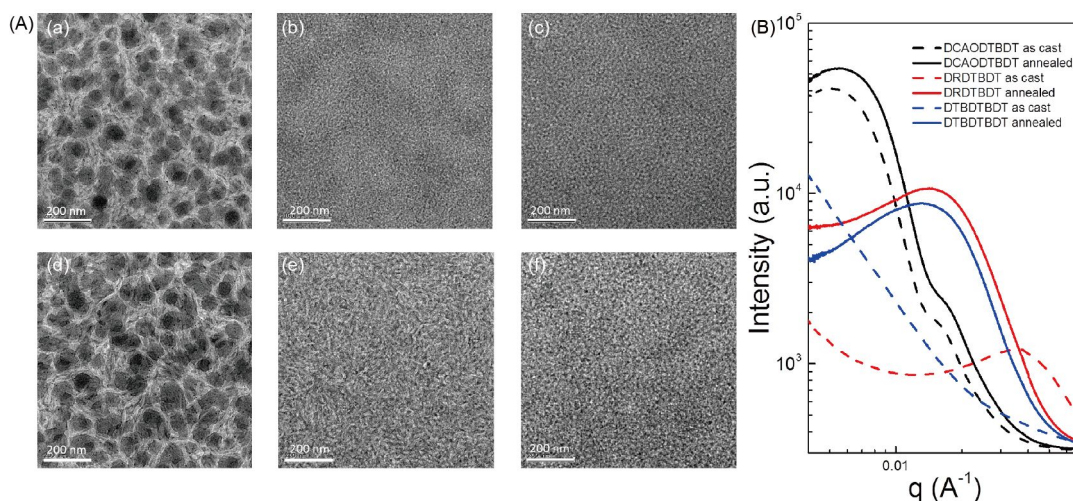


Figure 5 (A) TEM images of DCAODTBDT:PC₇₁BM, DRDTBDT:PC₇₁BM and DTBDTBDT:PC₇₁BM blend films without (a–c) and under optimized condition (d–f); (B) RSOS profiles of DCAODTBDT:PC₇₁BM, DRDTBDT:PC₇₁BM and DTBDTBDT:PC₇₁BM blend films (color online).

device performance was quit poor.

The charge carrier mobilities of DCAODTBDT:PC₇₁BM, DRDTBDT:PC₇₁BM and DTBDTBDT:PC₇₁BM blends are compared using the space-charge limited current (SCLC) method (Figure S3). The detailed parameters are recorded in Table S1. It is seen from these data that hole and electron mobilities are also influenced by the end acceptors in the studied molecules. All the blend films show low hole and electron mobilities without post treatment. After post treatment (by thermal or solvent annealing), DCAODTBDT, DRDTBDT and DTBDTBDT show hole mobility values of 8.35×10^{-5} , 1.04×10^{-4} and 9.26×10^{-5} cm² V⁻¹ s⁻¹, respectively. In addition, DRDTBDT also exhibits higher electron mobility (1.06×10^{-4} cm² V⁻¹ s⁻¹) than those of the devices with DCAODTBDT:PC₇₁BM (8.54×10^{-5} cm² V⁻¹ s⁻¹) and DTBDTBDT:PC₇₁BM (7.55×10^{-5} cm² V⁻¹ s⁻¹), implying that the charge carrier pathways are well developed in the active layer of the OPV device fabricated from the compound DRDTBDT.

4 Conclusions

Three dithienobenzodithiophene based A-D-A type small molecules with different end acceptor groups including octyl cyanoacetate, 3-octylrhodanine and thiobarbituric acid, named as DCAODTBDT, DRDTBDT and DTBDTBDT, have been designed and synthesized. The acceptor units have great impact not only on the band gaps and energy levels of these small molecules, but also obviously on the nanostructure of the blend films. With this, DCAODTBDT- and DTBDTBDT-based devices exhibit relatively low PCE of 4.83% and 3.39%, respectively, resulting mainly from the lower charge mobilities and not so well morphologies of the blend films. On the other hand, DRDTBDT, which has

rhodanine as the end moiety, exhibits higher charge mobilities, fine molecular ordering and well-developed fibrillary structure mixed with PC₇₁BM. Thus a high PCE of 8.34% is achieved for its devices, which is among the highest values for dithienobenzodithiophene based organic solar cells.

Acknowledgments This work was supported by the Ministry of Science and Technology (2014CB643502, 2016YFA0200200), and the Natural Science Foundation of China (21404060, 51422304, 91433101).

Conflict of interest The authors declare that they have no conflict of interest.

Supporting information The supporting information is available online at <http://chem.scichina.com> and <http://link.springer.com/journal/11426>. The supporting materials are published as submitted, without typesetting or editing. The responsibility for scientific accuracy and content remains entirely with the authors.

- 1 Peumans P, Yakimov A, Forrest SR. *J Appl Phys*, 2003, 93: 3693–3723
- 2 Service RF. *Science*, 2011, 332: 293–293
- 3 Zhou H, Yang L, You W. *Macromolecules*, 2012, 45: 607–632
- 4 Lu L, Yu L. *Adv Mater*, 2014, 26: 4413–4430
- 5 Li Y. *Acc Chem Res*, 2012, 45: 723–733
- 6 Li CZ, Chang CY, Zang Y, Ju HX, Chueh CC, Liang PW, Cho N, Ginger DS, Jen AKY. *Adv Mater*, 2014, 26: 6262–6267
- 7 Beaujuge PM, Fréchet JMJ. *J Am Chem Soc*, 2011, 133: 20009–20029
- 8 Hwang YJ, Courtright BAE, Ferreira AS, Tolbert SH, Jenekhe SA. *Adv Mater*, 2015, 27: 4578–4584
- 9 He Y, Chen HY, Hou J, Li Y. *J Am Chem Soc*, 2010, 132: 1377–1382
- 10 Eftaiha AF, Sun JP, Hill IG, Welch GC. *J Mater Chem A*, 2014, 2: 1201–1213
- 11 Kong J, Hwang IW, Lee K. *Adv Mater*, 2014, 26: 6275–6283
- 12 Zhou Y, Fuentes-Hernandez C, Shim J, Meyer J, Giordano AJ, Li H, Winget P, Papadopoulos T, Cheun H, Kim J, Fenoll M, Dindar A, Haske W, Najafabadi E, Khan TM, Sojoudi H, Barlow S, Graham S, Brédas JL, Marder SR, Kahn A, Kippelen B. *Science*, 2012, 336:

- 327–332
- 13 Duan C, Zhang K, Zhong C, Huang F, Cao Y. *Chem Soc Rev*, 2013, 42: 9071–9104
- 14 Dou L, You J, Hong Z, Xu Z, Li G, Street RA, Yang Y. *Adv Mater*, 2013, 25: 6642–6671
- 15 Dang MT, Wuest JD. *Chem Soc Rev*, 2013, 42: 9105–9126
- 16 Ameri T, Li N, Brabec CJ. *Energy Environ Sci*, 2013, 6: 2390–2413
- 17 You J, Dou L, Yoshimura K, Kato T, Ohya K, Moriarty T, Emery K, Chen CC, Gao J, Li G, Yang Y. *Nat Commun*, 2013, 4: 1446
- 18 Liu Y, Zhao J, Li Z, Mu C, Ma W, Hu H, Jiang K, Lin H, Ade H, Yan H. *Nat Commun*, 2014, 5: 5293–5300
- 19 Kang H, Kee S, Yu K, Lee J, Kim G, Kim J, Kim JR, Kong J, Lee K. *Adv Mater*, 2015, 27: 1408–1413
- 20 Chen JD, Cui C, Li YQ, Zhou L, Ou QD, Li C, Li Y, Tang JX. *Adv Mater*, 2015, 27: 1035–1041
- 21 Chen CC, Chang WH, Yoshimura K, Ohya K, You J, Gao J, Hong Z, Yang Y. *Adv Mater*, 2014, 26: 5670–5677
- 22 Zhang S, Ye L, Zhao W, Yang B, Wang Q, Hou J. *Sci China Chem*, 2015, 58: 248–256
- 23 Liu Y, Chen CC, Hong Z, Gao J, (Michael) Yang Y, Zhou H, Dou L, Li G, Yang Y. *Sci Rep*, 2013, 3: 3356
- 24 Kan B, Li M, Zhang Q, Liu F, Wan X, Wang Y, Ni W, Long G, Yang X, Feng H, Zuo Y, Zhang M, Huang F, Cao Y, Russell TP, Chen Y. *J Am Chem Soc*, 2015, 137: 3886–3893
- 25 Cui C, Guo X, Min J, Guo B, Cheng X, Zhang M, Brabec CJ, Li Y. *Adv Mater*, 2015, 27: 7469–7475
- 26 Gao K, Miao J, Xiao L, Deng W, Kan Y, Liang T, Wang C, Huang F, Peng J, Cao Y, Liu F, Russell TP, Wu H, Peng X. *Adv Mater*, 2016, 28: 4727–4733
- 27 Sun K, Xiao Z, Lu S, Zajaczkowski W, Pisula W, Hanssen E, White JM, Williamson RM, Subbiah J, Ouyang J, Holmes AB, Wong WWH, Jones DJ. *Nat Commun*, 2015, 6: 6013–6021
- 28 Coughlin JE, Henson ZB, Welch GC, Bazan GC. *Acc Chem Res*, 2014, 47: 257–270
- 29 Zhou J, Wan X, Liu Y, Zuo Y, Li Z, He G, Long G, Ni W, Li C, Su X, Chen Y. *J Am Chem Soc*, 2012, 134: 16345–16351
- 30 Chen Y, Wan X, Long G. *Acc Chem Res*, 2013, 46: 2645–2655
- 31 Bai H, Wang Y, Cheng P, Li Y, Zhu D, Zhan X. *ACS Appl Mater Interfaces*, 2014, 6: 8426–8433
- 32 Tang A, Zhan C, Yao J. *Chem Mater*, 2015, 27: 4719–4730
- 33 Shen S, Jiang P, He C, Zhang J, Shen P, Zhang Y, Yi Y, Zhang Z, Li Z, Li Y. *Chem Mater*, 2013, 25: 2274–2281
- 34 Anthony JE. *Chem Rev*, 2006, 106: 5028–5048
- 35 Feng H, Li M, Ni W, Liu F, Wan X, Kan B, Wang Y, Zhang Y, Zhang Q, Zuo Y, Yang X, Chen Y. *J Mater Chem A*, 2015, 3: 16679–16687
- 36 Son HJ, Lu L, Chen W, Xu T, Zheng T, Carsten B, Strzalka J, Darling SB, Chen LX, Yu L. *Adv Mater*, 2013, 25: 838–843
- 37 Wu JS, Cheng SW, Cheng YJ, Hsu CS. *Chem Soc Rev*, 2015, 44: 1113–1154
- 38 Chen HY, Hou J, Zhang S, Liang Y, Yang G, Yang Y, Yu L, Wu Y, Li G. *Nat Photon*, 2009, 3: 649–653
- 39 Liang Y, Xu Z, Xia J, Tsai ST, Wu Y, Li G, Ray C, Yu L. *Adv Mater*, 2010, 22: E135–E138
- 40 Liang Y, Yu L. *Acc Chem Res*, 2010, 43: 1227–1236
- 41 Price SC, Stuart AC, Yang L, Zhou H, You W. *J Am Chem Soc*, 2011, 133: 4625–4631
- 42 Huo L, Liu T, Sun X, Cai Y, Heeger AJ, Sun Y. *Adv Mater*, 2015, 27: 2938–2944
- 43 Wu Y, Li Z, Ma W, Huang Y, Huo L, Guo X, Zhang M, Ade H, Hou J. *Adv Mater*, 2013, 25: 3449–3455
- 44 Yun HJ, Lee YJ, Yoo SJ, Chung DS, Kim YH, Kwon SK. *Chem Eur J*, 2013, 19: 13242–13248
- 45 Wu Y, Li Z, Guo X, Fan H, Huo L, Hou J. *J Mater Chem*, 2012, 22: 21362–21365
- 46 Cheon YR, Kim YJ, Back JY, An T, Park CE, Kim YH. *J Mater Chem A*, 2014, 2: 16443–16451
- 47 Jung M, Seo D, Kwak K, Kim A, Cha W, Kim H, Yoon Y, Ko MJ, Lee DK, Kim JY, Son HJ, Kim BS. *Dyes Pigments*, 2015, 115: 23–34
- 48 Ni W, Wan X, Li M, Wang Y, Chen Y. *Chem Commun*, 2015, 51: 4936–4950
- 49 Kan B, Zhang Q, Li M, Wan X, Ni W, Long G, Wang Y, Yang X, Feng H, Chen Y. *J Am Chem Soc*, 2014, 136: 15529–15532
- 50 Li M, Ni W, Feng H, Wan X, Liu Y, Zuo Y, Kan B, Zhang Q, Chen Y. *Org Electron*, 2015, 24: 89–95
- 51 Li Z, He G, Wan X, Liu Y, Zhou J, Long G, Zuo Y, Zhang M, Chen Y. *Adv Energy Mater*, 2012, 2: 74–77
- 52 Zhou J, Zuo Y, Wan X, Long G, Zhang Q, Ni W, Liu Y, Li Z, He G, Li C, Kan B, Li M, Chen Y. *J Am Chem Soc*, 2013, 135: 8484–8487
- 53 He G, Li Z, Wan X, Liu Y, Zhou J, Long G, Zhang M, Chen Y. *J Mater Chem*, 2012, 22: 9173–9180
- 54 Long G, Wan X, Kan B, Liu Y, He G, Li Z, Zhang Y, Zhang Y, Zhang Q, Zhang M, Chen Y. *Adv Energy Mater*, 2013, 3: 639–646
- 55 Li CZ, Chueh CC, Yip HL, O'Malley KM, Chen WC, Jen AKY. *J Mater Chem*, 2012, 22: 8574–8578
- 56 Lu L, Luo Z, Xu T, Yu L. *Nano Lett*, 2013, 13: 59–64
- 57 Blom PWM, Mihailetschi VD, Koster LJA, Markov DE. *Adv Mater*, 2007, 19: 1551–1566
- 58 Guerrero A, Loser S, Garcia-Belmonte G, Bruns CJ, Smith J, Miyauchi H, Stupp SI, Bisquert J, Marks TJ. *Phys Chem Chem Phys*, 2013, 15: 16456–16462
- 59 Mandoc MM, Veurman W, Koster LJA, de Boer B, Blom PWM. *Adv Funct Mater*, 2007, 17: 2167–2173
- 60 Proctor CM, Kim C, Neher D, Nguyen TQ. *Adv Funct Mater*, 2013, 23: 3584–3594
- 61 He Z, Zhong C, Huang X, Wong WY, Wu H, Chen L, Su S, Cao Y. *Adv Mater*, 2011, 23: 4636–4643
- 62 Liu F, Gu Y, Shen X, Ferdous S, Wang HW, Russell TP. *Prog Polymer Sci*, 2013, 38: 1990–2052